



## Resistive Switching Characteristics of Solution-Processed Transparent TiO<sub>x</sub> for Nonvolatile Memory Application

Seungjae Jung,<sup>a</sup> Jaemin Kong,<sup>a</sup> Sunghoon Song,<sup>a</sup> Kwanghee Lee,<sup>a,b,c</sup>  
Takhee Lee,<sup>a,c</sup> Hyunsang Hwang,<sup>a,c,z</sup> and Sanghun Jeon<sup>d,z</sup>

<sup>a</sup>Department of Materials Science and Engineering, <sup>b</sup>Heeger Center for Advanced Materials, and <sup>c</sup>Department of Nanobio Materials and Electronics, Gwangju Institute of Science and Technology, Gwangju 500-712, Republic of Korea

<sup>d</sup>Samsung Advanced Institute of Technology, Devices Laboratory, Yongin, Gyeonggi 446-712, Republic of Korea

We propose a solution-processed transparent TiO<sub>x</sub>-based resistive switching random access memory (ReRAM) device. Electronically active TiO<sub>x</sub> was prepared by sol-gel spin coating of a titanium(IV) isopropoxide precursor on an indium tin oxide-coated glass. The prepared TiO<sub>x</sub> film is completely transparent in the visible range and has an amorphous structure. The fabricated TiO<sub>x</sub>-based ReRAM device exhibits distinct resistive switching under consecutive dc voltage sweeps of  $\pm 2$  V. The device also exhibits good memory performance, including fast switching speed with a pulse width of 1  $\mu$ s, stable pulse endurance over 1000 cycles, and excellent retention characteristics at up to 125°C. In addition, based on the  $\log I - \log V$  plot and X-ray photoelectron spectroscopy analysis, we postulate that the fabricated device is operated by the reversible formation/rupture of the conducting filament in the oxygen-deficient TiO<sub>x</sub> layer.

© 2010 The Electrochemical Society. [DOI: 10.1149/1.3489370] All rights reserved.

Manuscript submitted June 9, 2010; revised manuscript received August 16, 2010. Published September 23, 2010.

Recently, various types of nonvolatile memory devices, such as charge trap flash, spin-torque transfer, phase change, polymer, and resistive switching memory, have attracted considerable attention as alternatives to floating gate memory.<sup>1-5</sup> Among them, resistive switching random access memory (ReRAM) devices have been considered as one of the most promising candidates for next-generation nonvolatile memory devices because of their fast switching speed, low power operation, nondestructive readout, and remarkable scalability.<sup>5-7</sup> In particular, TiO<sub>2</sub>-based ReRAM devices have been widely investigated because of their relatively well-known operation mechanism and compatibility with the complementary metal-oxide-semiconductor process as compared with ternary or quaternary oxides such as doped SrZrO<sub>3</sub>, SrTiO<sub>3</sub>, (Sm,Ca)MnO<sub>3</sub>/(La,Sr)MnO<sub>3</sub>, and (Pr,Ca)MnO<sub>3</sub>.<sup>8-15</sup> Particularly, the solution processibility of TiO<sub>2</sub> has stimulated great interest from the viewpoints of ease in large-area fabrication, time-effective process, and low production cost.<sup>16,17</sup> Therefore, many researchers studied solution-processible TiO<sub>2</sub> and have recently reported that it could exhibit resistive switching characteristics.<sup>18-20</sup> They suggested that solution-processible TiO<sub>2</sub> could be a promising candidate for use in diverse applications such as memristors,<sup>18</sup> flexible ReRAMs,<sup>19</sup> and ReRAMs manufacturable by a simple manufacturing process.<sup>20</sup> However, information on the resistive switching mechanism and memory reliability of solution-processible TiO<sub>2</sub>, particularly with respect to its pulse endurance and high temperature retention characteristics, is inadequate from previous papers. In this study, we successfully fabricated a solution-processible, transparent TiO<sub>x</sub>-based ReRAM device and demonstrated its memory properties such as fast switching speed, stable pulse endurance over 1000 cycles, and excellent high temperature retention at up to 125°C. In addition, we investigated the resistive switching mechanism of the ReRAM device.

### Experimental

A TiO<sub>x</sub> sol-gel product was prepared according to the procedure described by Kim et al.<sup>21,22</sup> Titanium(IV) isopropoxide {Ti[OCH(CH<sub>3</sub>)<sub>2</sub>]<sub>4</sub>, Aldrich, 99.999%, 10 mL} was used as a precursor of the TiO<sub>x</sub> sol-gel product. The precursor was mixed with 2-methoxyethanol (CH<sub>3</sub>OCH<sub>2</sub>CH<sub>2</sub>OH, Aldrich, 99.9 + %, 50 mL) and ethanolamine (H<sub>2</sub>NCH<sub>2</sub>CH<sub>2</sub>OH, Aldrich, 99 + %, 5 mL) in a three-necked flask equipped with a condenser, a thermometer, and

an argon-gas inlet/outlet. Then, the mixed solution was heated in a silicone-oil bath with stirring to 80°C for 2 h, followed by heating to 120°C for 1 h in argon ambient. Subsequent to the two-step heating process, the product was cooled down to room temperature and was diluted with isopropyl alcohol (IPA). For ReRAM device fabrication, a glass substrate coated with indium tin oxide (ITO) was cleaned by mechanical cleaning with detergent and by successive wet cleaning through ultrasonication for 15 min each in deionized water, acetone, and IPA. Further, the ITO-coated glass substrate was dried in a vacuum oven at 100°C for 4 h, followed by UV/O<sub>3</sub> surface treatment. The substrate was spin-coated directly by the TiO<sub>x</sub> precursor solution and then hydrolyzed at room temperature for 1 h in air (TiO<sub>x</sub>  $\sim$  50 nm). Finally, an Al top electrode and Pt capping layer with an area of 100  $\times$  100  $\mu$ m were formed by shadow mask and postannealing was implemented at 150°C in N<sub>2</sub> ambient.

### Results and Discussion

Figure 1a shows the transmittance of TiO<sub>x</sub> on fused silica as a function of the wavelength of the incident beam. The optical bandgap  $E_g$  can be determined using the absorption coefficient and has been investigated by studying the relation  $(\alpha h\nu)^2$  vs  $h\nu$ , considering the direct allowed transition of TiO<sub>2</sub>, as shown in Fig. 1b.<sup>23,24</sup> The optical bandgap can be obtained by extrapolating the linear portion of the graph to the photon energy;  $E_g = 3.85$  eV. This value indicates that the prepared TiO<sub>x</sub> film is completely transparent to the human eye. Because the TiO<sub>x</sub> film was prepared at room temperature and annealed in N<sub>2</sub> at 150°C (much below the crystallization temperatures (T<sub>c</sub>) of the two major phases, anatase and rutile, T<sub>c</sub>  $\sim$  400°C), as expected, the prepared TiO<sub>x</sub> film was confirmed to be amorphous by X-ray diffraction analysis (Fig. 2).

Figure 3 shows the current-voltage ( $I$ - $V$ ) curves of the Al/TiO<sub>x</sub>/ITO metal-insulator-metal device that exhibits bipolar (antisymmetric) switching behavior under the dc voltage sweep. During all the electrical measurement, a voltage was applied to the Al top electrode, and the ITO bottom electrode was electrically grounded. Before measuring the resistive switching characteristics of the device, an initial forming process was required. When a positive bias was first applied to the Al top electrode, the forming process occurred. In contrast, when a positive bias was applied to the ITO bottom electrode first, the forming process was not observed and the device did not exhibit any resistive switching at all. This voltage polarity dependence of the forming process can be explained by the much stronger tendency of Al to oxidize compared to ITO.<sup>25</sup> Then,

<sup>z</sup> E-mail: hwanghs@gist.ac.kr; sanghun1.jeon@samsung.com

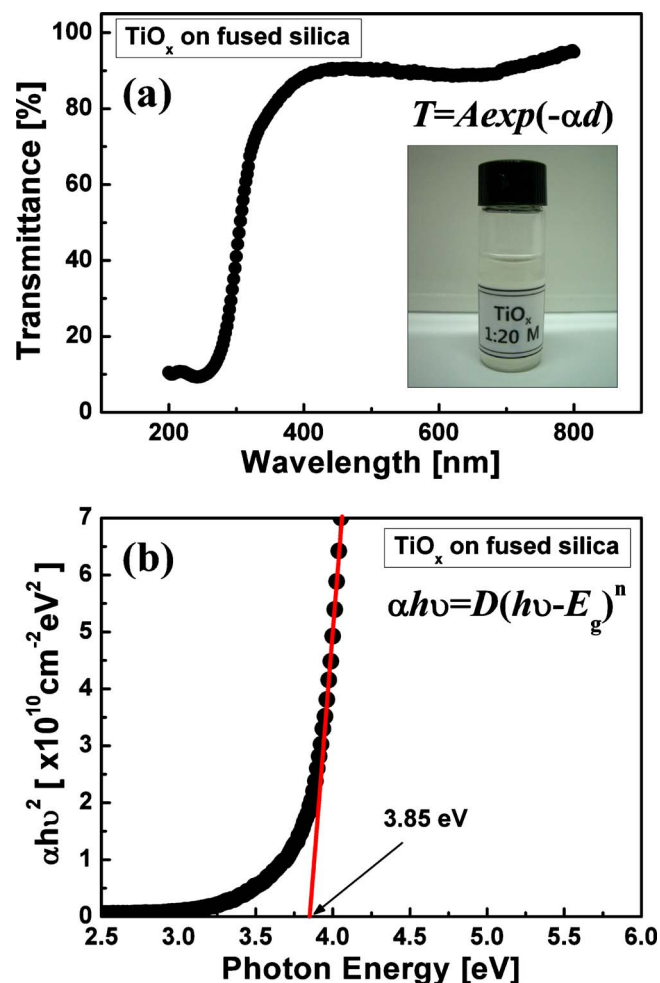


Figure 1. (Color online) (a) Optical transmittance and (b) calculated optical bandgap for direct allowed transition of the solution-processed  $\text{TiO}_x$  film.

as we apply a positive voltage greater than the threshold voltage of  $\sim 1.0$  V, the device switches (“set”) from its high resistance state (HRS) to a low resistance state (LRS). The current is limited by the compliance current of 1 mA of the control circuit. When we apply a

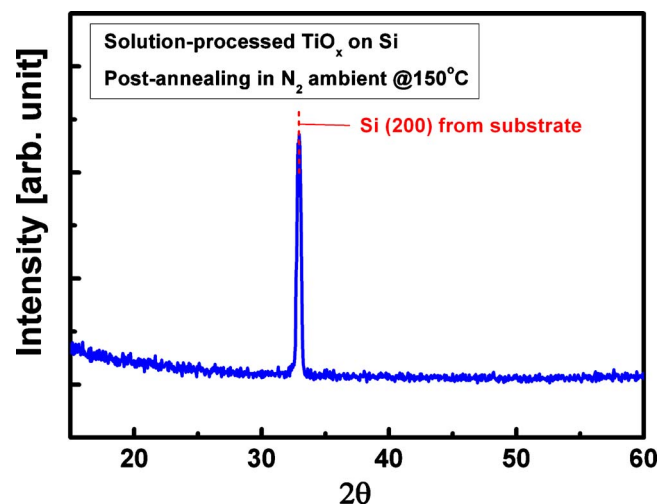


Figure 2. (Color online) X-ray diffraction pattern of the solution-processed  $\text{TiO}_x$  film. The diffraction peak from Si substrate is only observed at  $\sim 33^\circ$ .

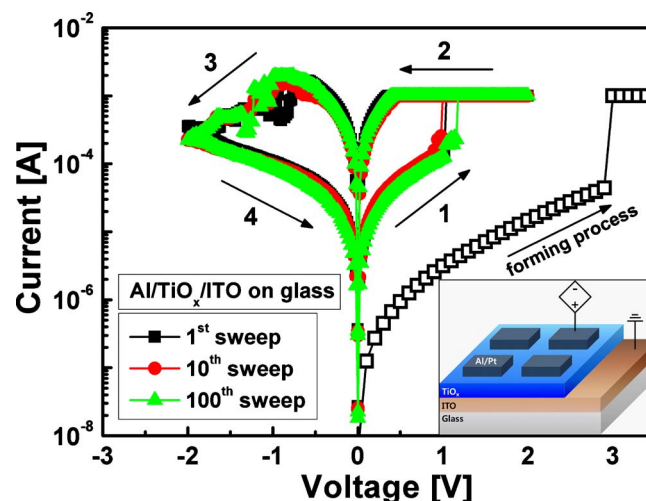


Figure 3. (Color online) Typical  $I$ - $V$  hysteresis curves of the  $\text{TiO}_x$ -based ReRAM device. The initial forming process is also represented.

negative voltage below a certain voltage of approximately  $-1.0$  V, the device switches back from LRS to HRS. This “reset” process to HRS occurs as a result of reverse voltage polarity. This switching phenomenon is called the bipolar switching behavior. After an initial electroforming step at  $+3$  V, the fabricated device exhibits stable switching behavior over 100 times under consecutive dc voltage sweeps of  $\pm 2$  V. The fabricated cell did not show the unipolar resistive switching behavior. If the top electrode is changed to Pt, the unipolar switching was observed. However, the  $I$ - $V$  characteristic was very unstable and no continuous resistive switching was obtained (data not shown here).

In addition, the two different resistance states (HRS and LRS) were monitored as a function of the pulse duration at a pulse voltage of  $\pm 2$  V, as shown in Fig. 4. The fabricated ReRAM device demonstrates fast switching. Although the onset of decreasing set/reset resistance ratio was observed at 500 ns, the ratio remains nearly constant for a duration of up to 1  $\mu\text{s}$ .

For further analysis, the retention characteristic of the device was measured at various temperatures to verify the temperature-dependent stability in HRS and LRS. As seen in Fig. 5, no noticeable degradation can be observed in the current magnitude at measurement temperatures ranging from 25 to 125°C for  $10^4$  s,

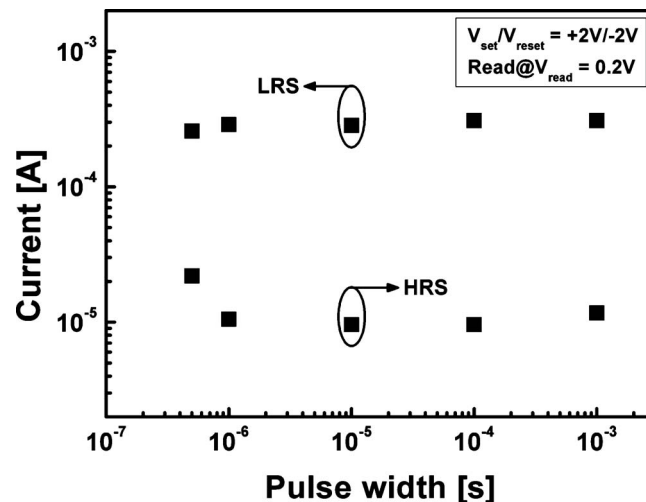
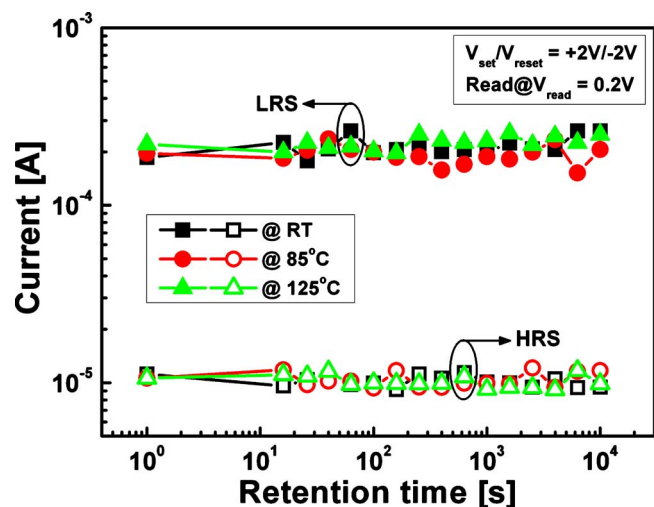


Figure 4. HRS and LRS as a function of the pulse duration at a pulse voltage of  $\pm 2$  V. Both resistance states remain stable at up to 1  $\mu\text{s}$ .



**Figure 5.** (Color online) Retention characteristics of the  $\text{TiO}_x$ -based ReRAM device at various temperatures ranging from 25 to 125°C. No significant degradation was observed up to  $10^4$  s.

indicating that the formed conducting filaments are stable up to a high temperature of 125°C, and the formation of any tiny filament causing a switch to LRS is not triggered until measurement temperatures of 125°C. This implies that the solution-based process presented in this study can produce an effective, electronically active  $\text{TiO}_x$  layer suitable for ReRAM devices and such  $\text{TiO}_x$ -based ReRAM devices are superior to  $\text{Al}_2\text{O}_3$ - and  $\text{CuO}$ -based devices, which exhibit unstable retention characteristics at 125°C.<sup>26,27</sup> Another reliability test was performed, in which a pulse endurance test was employed to evaluate the electrical stability in both resistance states at a reading voltage of 0.2 V ( $V_{\text{set}}/V_{\text{reset}} = +2$  V, 10  $\mu\text{s}/-2$  V, 1  $\mu\text{s}$ ). Even if there is a slight fluctuation in the current magnitudes of both resistance states, these states are continuously stable, maintaining HRS and LRS over 1000 cycles, as shown in Fig. 6. For a ReRAM device with the solution-processed  $\text{TiO}_x$  layer, these values are superior to those reported previously.<sup>18-20</sup>

For understanding the conduction mechanism of  $\text{TiO}_x$  in both HRS and LRS, the  $\log I - \log V$  characteristics were plotted, as shown in Fig. 7. The  $\log I - \log V$  plot of LRS is linearly fitted to

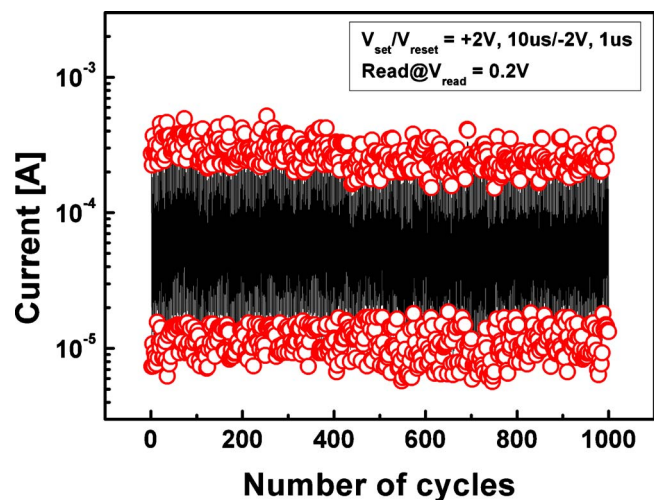


**Figure 6.** (Color online) Cycling endurance characteristics of the  $\text{TiO}_x$ -based ReRAM device measured by consecutive voltage pulse ( $V_{\text{set}}/V_{\text{reset}} = +2$  V, 10  $\mu\text{s}/-2$  V, 1  $\mu\text{s}$ ). The resistance values of both states were extracted at a reading voltage of 0.2 V.

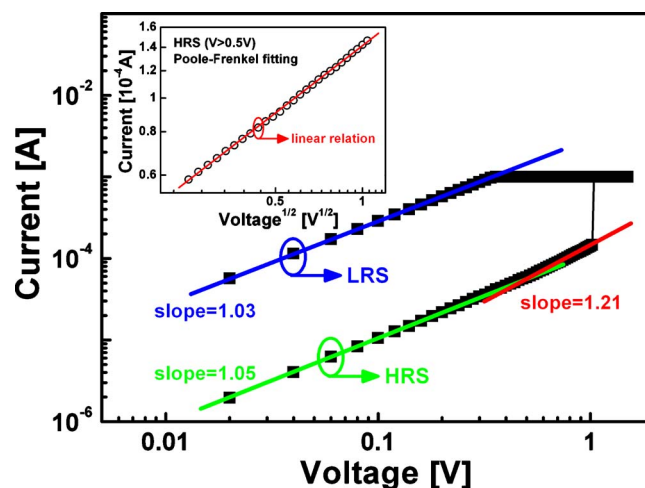


**Figure 7.** (Color online) The  $\log I - \log V$  plot of HRS and LRS of the  $\text{TiO}_x$ -based ReRAM device. The inset depicts the PF emission fitting at high voltage region ( $>0.5$  V) in the HRS.

a line with slope 1.0, implying that the charge transport mechanism in LRS follows ohmic conduction. The conduction behavior in HRS can be explained by ohmic conduction at the low voltage region because the slope of approximately 1 remains valid at the low voltage region. However, at the high voltage region ( $>0.5$  V), the conduction mechanism in HRS is completely different because the slope of the fitted line increases to 1.21. This nonlinear relation of the  $\log I - \log V$  plot might be attributable to the Poole-Frenkel (PF) emission. According to the PF conduction, a plot of  $\log I$  vs  $V^{1/2}$  has a linear relation, as shown in the inset of Fig. 7. Defect density is often used as the criterion to distinguish between amorphous and crystalline states, and there is a large number of defects in amorphous  $\text{TiO}_x$ .<sup>28</sup> Thus, once the charges trapped in these trapping sites obtain sufficient energy from a high electric field or high temperature, they can overcome the energy barrier of the traps in amorphous  $\text{TiO}_x$  or the interface of  $\text{TiO}_x$  and the Al electrode can contribute to electrical conduction. This result is consistent with that of a previous paper that investigated amorphous  $\text{TiO}_x$ -based ReRAM devices.<sup>29</sup>

Based on the analysis described above, the charge transport mechanism of the fabricated  $\text{TiO}_x$ -based ReRAM device in both states can be explained by the well-known conductive filament model. Some existing defects in the prepared  $\text{TiO}_x$  film connect with each other and contribute to ohmic conduction at low voltage. However, with increasing voltage, the conduction is dominated by the PF emission, which is directly associated with the traps in amorphous  $\text{TiO}_x$  films. Once the electric field through the  $\text{TiO}_x$  film reaches a specific value, it leads to the formation of a conductive filament throughout the film. Therefore, large current flows through the conductive path and conduction in LRS is explained by ohmic behavior. In contrast, in the reset process from LRS to HRS, most of the conductive filaments are disrupted due to the reverse bias. As a consequence, the electric conduction decreases suddenly, causing the switch to HRS. The area dependence of HRS and LRS on the current was also observed, as depicted in Fig. 8. Showing the area dependence of two resistance states is very useful to prove the filamentary switching behavior of ReRAM devices. As described in Fig. 8, LRS is not affected by the active area of the ReRAM device. Because the formation of a conducting path (first filament) could prevent the generation of other conducting paths, the LRS current is independent of the device size. In contrast, the HRS current is proportional to the active area of our ReRAM device because the HRS current is dominantly determined by the leakage current. Therefore, the switching mechanism of our ReRAM device is the formation/rupture of the conducting filament.

To investigate the origin of defects in amorphous  $\text{TiO}_x$ , which

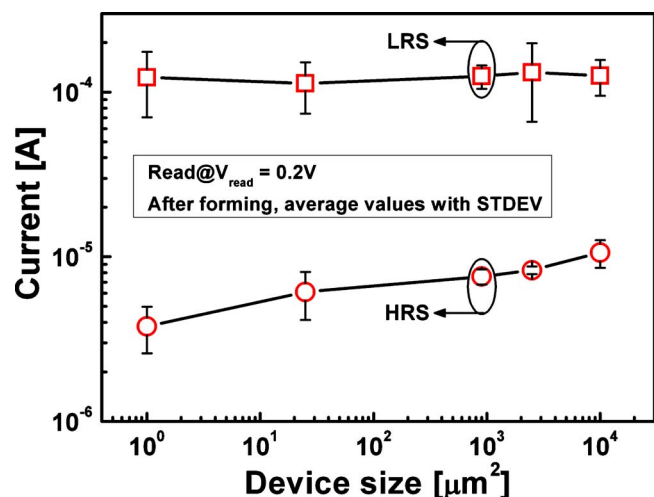


**Figure 8.** (Color online) The current of HRS and LRS as a function of device size.

contribute to conduction, X-ray photoelectron spectroscopy (XPS) analysis was performed. Figure 9 shows the XPS Ti 2p spectrum, which was resolved into two Ti-related peaks  $Ti^{4+}$  (binding energy = 459.0 eV) and  $Ti^{3+}$  (binding energy = 457.6 eV).<sup>30</sup> Here, the broad shoulder peak in the spectrum can be assigned to  $Ti^{3+}$ .  $Ti^{3+}$  is related to the oxygen-deficient state in the  $TiO_x$  film.<sup>15,20</sup> Taking into account the results inferred from the  $\log I - \log V$  plot and XPS, the migration of these oxygen vacancies caused by the external electric field in the solution-processed amorphous  $TiO_x$  film could have induced reversible formation/rupture of the conductive filament, bringing about stable filamentary switching behavior,<sup>15,20,29,31-35</sup> hence, the solution-processed  $TiO_x$ -based ReRAM device fabricated in this study exhibited good memory performance.

In summary, the effectiveness of a ReRAM device with a solution-processed transparent  $TiO_x$  layer was successfully demonstrated. The active  $TiO_x$  film was spin-coated on glass and fabricated by sol-gel chemistry using a titanium(IV) isopropoxide precursor.

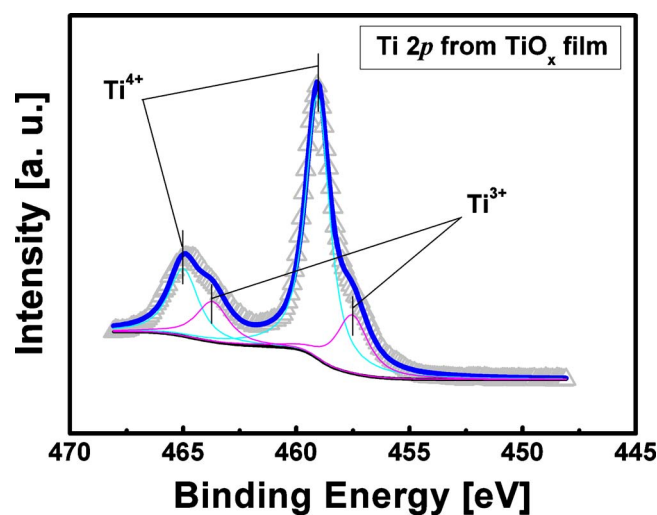


**Figure 9.** (Color online) Ti 2p portion of the XPS spectra of the solution-processed  $TiO_x$  film. The binding energies of Ti 2p<sub>1/2</sub> and Ti 2p<sub>3/2</sub> were measured after postannealing at 150°C.

The prepared  $TiO_x$  film was completely transparent and amorphous. Moreover, the  $TiO_x$ -based ReRAM device exhibited good memory performance, including stable dc resistive switching characteristic over 100 times, fast switching speed with pulse widths of up to 500 ns, stable pulse endurance under the condition  $V_{set}/V_{reset} = +2$  V, 10  $\mu s$ /-2 V, 1  $\mu s$  over 1000 cycles, and excellent retention characteristics up to temperatures of 125°C. In addition, based on the  $\log I - \log V$  plot and XPS analysis, the switching mechanism of the fabricated device is the reversible formation/rupture of the conducting filament. This resulted from the migration of the oxygen vacancies in the oxygen-deficient amorphous  $TiO_x$  layer.

#### Acknowledgment

This work was supported by the National Research Laboratory (NRL) Programs of the Korea Science and Engineering Foundation (KOSEF). K. Lee and J. Kong acknowledge the National Research Foundation of Korea (KRF) grant funded by the Ministry of Education, Science and Technology (MEST) of Korea (No. 20090093869).

Gwangju Institute of Science and Technology assisted in meeting the publication costs of this article.

#### References

1. Y. Yang, A. Purwar, and M. H. White, *Solid-State Electron.*, **43**, 2025 (1999).
2. M. Hosomi, H. Yamagishi, T. Yamamoto, K. Bessho, Y. Higo, K. Yamane, H. Yamada, M. Shoji, H. Hachino, C. Fukumoto, et al., *Tech. Dig. - Int. Electron Devices Meet.*, **2005**, 459.
3. G. Servalli, *Tech. Dig. - Int. Electron Devices Meet.*, **2009**, 113.
4. J. Ouyang, C.-W. Chu, C. R. Szmanda, L. Ma, and Y. Yang, *Nature Mater.*, **3**, 918 (2004).
5. S. Q. Liu, N. J. Wu, and A. Ignatiev, *Appl. Phys. Lett.*, **76**, 2749 (2000).
6. International Technology Roadmap for Semiconductors (ITRS) (2008).
7. R. Waser and M. Aono, *Nature Mater.*, **6**, 833 (2007).
8. A. Beck, J. G. Bednorz, Ch. Gerber, C. Rossel, and D. Widmer, *Appl. Phys. Lett.*, **77**, 139 (2000).
9. D. Seong, M. Jo, D. Lee, and H. Hwang, *Electrochem. Solid-State Lett.*, **10**, H168 (2007).
10. A. Sawa, T. Fujii, M. Kawasaki, and Y. Tokura, *Appl. Phys. Lett.*, **88**, 232112 (2006).
11. D. Seong, J. Park, N. Lee, M. Hasan, S. Jung, H. Choi, J. Lee, M. Jo, W. Lee, S. Park, et al., *Tech. Dig. - Int. Electron Devices Meet.*, **2009**, 101.
12. W. Chang, Y. Ho, T. Hsu, F. Chen, M. Tsai, and T. Wu, *Electrochem. Solid-State Lett.*, **12**, H135 (2009).
13. B. Choi, S. Choi, K. Kim, Y. Shin, C. Hwang, S. Hwang, S. Cho, S. Park, and S. Hong, *Appl. Phys. Lett.*, **89**, 012906 (2006).
14. K. Kim, B. Choi, B. Koo, S. Choi, D. Jeong, and C. Hwang, *Electrochem. Solid-State Lett.*, **9**, G343 (2006).
15. J. Yang, M. Pickett, X. Li, D. Ohlberg, D. Stewart, and R. Williams, *Nat. Nanotechnol.*, **3**, 429 (2008).
16. J. Kim, K. Lee, N. E. Coates, D. Moses, T. Nguyen, M. Dante, and A. J. Heeger, *Science*, **317**, 222 (2007).
17. R. J. Tseng, J. Huang, J. Ouyang, R. B. Kaner, and Y. Yang, *Nano Lett.*, **5**, 1077 (2005).
18. N. Gergel-Hackett, B. Hamadani, B. Dunlap, J. Suehle, C. Richter, C. Hacker, and D. Gundlach, *IEEE Electron Device Lett.*, **30**, 706 (2009).
19. J. Yun, K. Cho, B. Park, B. Park, and S. Kim, *J. Mater. Chem.*, **19**, 2082 (2009).
20. C. Lee, I. Kim, W. Choi, H. Shin, and J. Cho, *Langmuir*, **25**, 4274 (2009).
21. J. Kim, S. Kim, H. Lee, K. Lee, W. Ma, X. Gong, and A. Heeger, *Adv. Mater.*, **18**, 572 (2006).
22. S. Cho, K. Lee, and A. J. Heeger, *Adv. Mater.*, **21**, 1941 (2009).
23. G. Li, L. Yang, Y. Jin, and L. Zhang, *Thin Solid Films*, **368**, 164 (2000).
24. N. Serpone, D. Lawless, and R. Khairutdinov, *J. Phys. Chem.*, **99**, 16646 (1995).
25. H. Shima, F. Takano, H. Muramatsu, H. Akinaga, Y. Tamai, I. Inque, and H. Takagi, *Appl. Phys. Lett.*, **93**, 113504 (2008).
26. S. Kim and Y. Choi, *Appl. Phys. Lett.*, **92**, 223508 (2008).
27. H. B. Lv, M. Yin, X. F. Fu, Y. L. Song, L. Tang, P. Zhou, C. H. Zhao, T. A. Tang, B. A. Chen, and Y. Y. Lin, *IEEE Electron Device Lett.*, **29**, 309 (2008).
28. C. Chang and S. M. Sze, *ULSI Technology*, p. 178, McGraw-Hill International, New York (1996).
29. H. Jeong, J. Lee, M. Ryu, and S. Choi, *Phys. Status Solidi (RRL)*, **4**, 28 (2010).
30. C. D. Wagner, A. V. Naumkin, A. Kraut-Vass, J. W. Allison, C. J. Powell, and J. R. Rumble, *NIST X-Ray Photoelectron Spectroscopy Database*, version 3.5 (web version), National Institute of Standards and Technology, Gaithersburg, MD (2003).
31. D. Kwon, K. Kim, J. Jang, J. Jeon, M. Lee, G. Kim, X. Li, G. Park, B. Lee, S. Han, et al., *Nat. Nanotechnol.*, **5**, 148 (2010).
32. L. Yu, S. Kim, M. Ryu, S. Choi, and Y. Choi, *IEEE Electron Device Lett.*, **29**, 331 (2008).
33. H. Jeong, J. Lee, S. Choi, and J. Kim, *Appl. Phys. Lett.*, **95**, 162108 (2009).